ELSEVIER

Surface Science 458 (2000) 34–52

surface science

www.elsevier.nl/locate/susc

Structure and growth of 4-methyl-4′-mercaptobiphenyl monolayers on Au(111): a surface diffraction study

T.Y.B. Leung [a,1], P. Schwartz [a,2], G. Scoles [a,*], F. Schreiber [b], A. Ulman [c]

[a] *Department of Chemistry, Princeton University, Princeton, NJ 08544, USA*
[b] *Max-Planck-Institut für Metallforschung, Heisenbergstr. 1, 70569 Stuttgart, Germany*
[c] *Department of Chemistry, Polytechnic University, Brooklyn, NY 11201, USA*

Received 28 September 1999; accepted for publication 1 January 2000

Abstract

In an attempt to quantify the role played by the rigidity of the molecular backbone on the self-assembly process, monolayers of 4-methyl-4′-mercaptobiphenyl assembled on Au(111) were characterized by grazing incidence X-ray diffraction and low-energy atomic beam diffraction. Two phases of different density were observed. In the low-density 'striped' phase, the diffraction pattern is consistent with a commensurate rectangular $(8 \times 2\sqrt{3})$ surface lattice. Systematic absences and the intensity modulation in the diffraction pattern suggest that the structure can be composed by staggered molecular rows arranged in a head-to-head orientation with their molecular axes close to the surface. The diffraction pattern of the high-density phase can be described by a commensurate $(\sqrt{3} \times \sqrt{3})R30^\circ$ surface lattice. The measured intensity variation along the (1, 1) Bragg rod is consistent with a tilt angle of at most 19° from the surface normal. Therefore, both similarities and differences with the diffraction patterns of the low-density phase and the high-density phase of the monolayers of *n*-alkanethiol on Au(111) have been detected. The thermal behavior of the monolayers of 4-methyl-4′-mercaptobiphenyl was also examined. Both phases are found to be thermally more stable than the corresponding phases of monolayers of *n*-alkanethiols. Finally, the growth behavior of the monolayers of 4-methyl-4′-mercaptobiphenyl was investigated and various growth protocols were tried. Compared with the case of *n*-alkanethiol monolayers, the high-density phase of the monolayers of 4-methyl-4′-mercaptobiphenyl is more difficult to prepare.

Keywords: Atom–solid scattering and diffraction – elastic; Chemisorption; Gold; Low index single crystal surfaces; Self-assembly; X-ray diffraction

1. Introduction

For almost two decades, self-assembled monolayers (SAMs) of *n*-alkanethiol on gold have been widely studied in the scientific community because of their technological relevance and scientific importance [1–3]. The self-assembly process involves various interactions, including the headgroup–substrate interaction, the endgroup–substrate interaction, the chain–chain interaction and the endgroup–endgroup interaction [4–7]. With substantial effort, aimed mostly at the structural characterization of the monolayers, a better understanding of the headgroup–substrate and the endgroup–endgroup interactions in the assembly

* Corresponding author. Fax: +1-609-258-6746.
E-mail address: gscoles@pucc.princeton.edu (G. Scoles)
[1] Present address: Department of Chemistry, University of Illinois, Urbana, IL 61801, USA.
[2] Present address: Chemistry Department, Northwestern University, 2145 Sheridan Road, Evanston, IL 60628-3113, USA.

0039-6028/00/$ - see front matter
PII: S0039-6028(00)00385-X

process has been obtained [8–20]. The impact of the nature and the rigidity of the molecular backbone on the assembly process is, however, not well understood, as reports focusing on this subject have appeared less frequently in the literature [21–29].

In a previous study by Creager and Steiger [21] of the monolayers of 4-mercaptobenzoic acid on gold, it was concluded that the rigidity of the phenyl rings prevented intermolecular H-bonding and the dimerization of the carboxylic groups. There have also been reports on the effect of the constraint of the backbone packing onto the self-assembly. After using scanning tunneling microscopy (STM) and considering the van der Waals dimension of the aromatic groups, Sita and co-workers [22] propose that monolayers of conjugated arylthiol derivatives may adopt a herringbone packing. A previous study carried out at Princeton [23] on monolayers of partly perfluorinated thiols leads to an incommensurate structure that can be attributed to a balance of the headgroup–substrate interaction and the packing constraints of the bulky fluorinated backbone. There are also reports in the literature on monolayers of 4-mercaptobiphenyl, which is very similar to the molecule used in the present study [4-methyl-4′-mercaptobiphenyl, $CH_3-C_6H_4-C_6H_4-SH$, (MMB)] [24,25]. The structure of these monolayers and the role of the biphenyl units in the assembly process, however, have not been unequivocally determined.

Since most of the previous studies used macroscopic or indirect characterization tools, a molecular-level understanding of the effect of the molecular backbone is still lacking. Several questions pertaining to this issue can be posed. As the structure is determined by the overall balance of all interactions involved in the self-assembly process, how does the nature of the molecular backbone affect the structure of the monolayers? In order to tune the properties of the monolayers in a controlled fashion, we need to know how the properties correlate with the structures. Furthermore, a recent multi-technique study on aliphatic thiol monolayers carried out in our laboratory has mapped their growth in its relationship to the multiple energy scales present in the system [30]. As the entropic contribution and the intermolecular interactions are strongly related to the rigidity of the molecular backbone, it is highly desirable to understand how the nature of the molecular backbone influences the growth behavior of the monolayers.

To answer these questions, in situ, direct and quantitative techniques such as grazing incidence X-ray diffraction (GIXD) and low-energy atomic diffraction (LEAD) are called for [4]. GIXD provides an accurate measurement of the lattice dimensions and the symmetry of the structure within the surface plane and is able to measure the average domain size of the monolayers with good accuracy. Thus, a quantitative measure of the quality of the monolayers can be obtained. Using this technique, the thermal behavior and the growth of the monolayers can be studied in situ and in real time, and the correlation between the thermal history of the sample and its structure can be determined [30,31]. LEAD is more surface-specific and can probe with high sensitivity the presence of early growth phases (in which the molecules may lie down on the surface [32,33]) and of possible superlattices, especially when these produce a change in the surface corrugation at the monolayer surface–vacuum interface [34].

In order to study the role of the molecular backbones in the assembly process, MMB was chosen for this study. Compared with the alkyl chains of the *n*-alkanethiols, the biphenyl units of MMB are much more rigid and have a different shape. On the other hand, MMB has similar length to a fully extended *n*-decanethiol (the most thoroughly studied system so far) and shares with this molecule both headgroup and endgroup. SAMs and mixed SAMs of 4′-substituted, 4-mercaptobiphenyl derivatives have been studied in recent years [35–38]. It was found that they provide stable model surfaces for the studies of wetting [35], owing to their rigidity and the lack of conformational disorder. It was also observed that the composition of mixed SAMs in equilibrium depends on the polarity of the solvent from which they were assembled [37] and that the kinetics of SAM formation depends strongly on intermolecular dipolar interactions [38].

In this report, the results of a comprehensive diffraction study of the structures, the thermal behavior, and the growth behavior of monolayers of MMB on Au(111) are presented. Two phases of different density were observed. In a low-density phase, the molecules are believed to assemble in rows lying down on the surface. A second, high-density, phase is thought to be composed of a hexagonal arrangement of molecules, which are aligned along the surface normal. We denote the low-density phase as the 'striped' phase and the high-density phase as the 'hexagonal' phase. The striped phase and the hexagonal phase are also observed in monolayers of *n*-alkanethiol on Au(111) (hereafter denoted as C_n, where n is the number of carbons in the alkyl chain). However, interesting differences were found.

Annealing experiments show that both phases of MMB monolayers are thermally more stable than the corresponding phases of C_n. In addition, the growth behavior of MMB monolayers was investigated and different growth protocols were attempted. Unlike the case of C_n where the hexagonal phase can be grown reliably and reproducibly, the hexagonal phase of MMB monolayers has only been observed a few times. This disparity between MMB monolayers and C_n is discussed in terms of the energetics of the various interactions involved and the role of the molecular backbone is addressed.

The outline of this paper is as follows. The experimental details are described in the Section 2. Then, the structural results (Section 3), the thermal properties (Section 4) and the growth behavior (Section 5) of MMB monolayers are presented. In Section 6, the impact of the molecular backbone in the self-assembly process is discussed by comparing the results gathered here with our knowledge of C_{10}. A summary of the results and the conclusions is given in Section 7.

2. Experimental details

2.1. Sample preparation

Single crystal Au(111) substrates were used in order to examine the intrinsic properties of the monolayers on well-defined surfaces. Substrates were cleaned by repeated cycles of argon-ion bombardment and annealing. The cleanliness of the substrates is manifested by the observation of the well-known $(22\times\sqrt{3})$ reconstruction [39]. The synthesis of MMB was carried out by palladium-catalyzed coupling of 4-*t*-butylmercaptophenyl magnesium bromide with 4-iodotoluene. The *t*-butyl protecting group was removed using Hg^{2+}. Details will be published elsewhere [40].

Monolayers were prepared by a variety of growth conditions. They include the following: (i) conventional liquid-phase deposition [18,19]; (ii) in vacuo vapor-phase deposition at different substrate temperatures [30]; and (iii) in an 'alkane-assisted' mode in which in vacuo vapor-phase deposition was carried out on a pre-adsorbed layer of hydrocarbon molecules [41]. In the conventional liquid-phase deposition, a clean substrate was incubated in an ethanolic solution of thiol at room temperature. Concentrations ranged from 0.01 to 1 mM and the deposition time ranged from 20 min to 7 days. Prior to installation into the vacuum chamber, the samples were rinsed several times with solvent.

For in vacuo vapor-phase deposition, the gas manifolds connecting to the thiol source were pumped out for at least 30 min in order to remove any volatile impurities. Deposition was carried out by exposing a clean substrate to the vapor of MMB. As the thiol in the present study has a rather low vapor pressure, the impingement rate at the sample is increased by using a heatable doser tube that can generate a molecular beam of thiol. Owing to technical reasons, the diffraction intensity was not measured at a dosing time less than 3 min. The diffraction intensity of the low density striped phase was found to remain typically unchanged after 3 min of exposure, i.e. it is suggested that samples reach full coverage in 3 min of dosing time. The dosing pressure of the thiol at the sample is derived to be at least 10^{-8} Torr. The substrate temperature ranged from 285 to 433 K. In the 'alkane-assisted' growth mode, the substrate temperature ranged from 288 to 310 K. For this study, *n*-dodecane and *n*-octadecane were purchased from Aldrich Chemical Company (nominal purity: 99%). They were used as received.

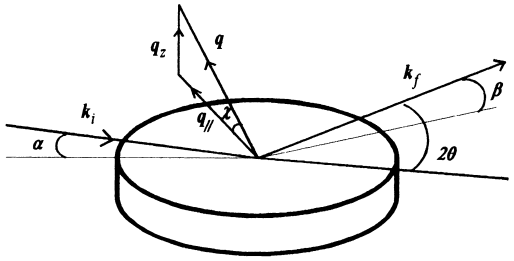

Fig. 1. A schematic diagram of the scattering geometry used in the GIXD measurements.

2.2. GIXD

Overviews of the technique and the experimental set-up have been described elsewhere [4–6]. Here, the technique is outlined and the information that is specific for this study is highlighted. The scattering geometry used is shown in Fig. 1. The total momentum transfer $\boldsymbol{q}$ and the perpendicular momentum transfer $\boldsymbol{q}_z$ are:

$$\boldsymbol{q} = \boldsymbol{k}_\mathrm{f} - \boldsymbol{k}_\mathrm{i} \tag{1}$$

$$|\boldsymbol{q}| = 2|\boldsymbol{k}_\mathrm{i}| \sin\left(\frac{2\theta}{2}\right) \tag{1a}$$

$$|\boldsymbol{q}_z| = |\boldsymbol{k}_\mathrm{i}|(\sin\alpha + \sin\beta), \tag{2}$$

where $\boldsymbol{k}_\mathrm{i}$ and α are the incidentwave vector and angle, and $\boldsymbol{k}_\mathrm{f}$ and β are the exit wave vector and angle. Typically, in-plane diffraction patterns are obtained by measuring the intensity of scattered X-rays as a function of the azimuthal angle ϕ and the parallel momentum transfer $\boldsymbol{q}_\parallel$. For two-dimensional surveys, $\boldsymbol{q}_z$ is usually kept at a small value. The unit mesh dimensions and the symmetry of the monolayers can then be determined from the diffraction pattern.

All the measurements shown were taken at a wavelength of 1.130 Å. The resolution was set by the detector slits and is a function of the diffractometer angles [42]. For the in-plane diffraction measurements, $\delta q_\parallel$ ranged from 0.0156 $\mathrm{Å}^{-1}$ (at small angle χ) to 0.0213 $\mathrm{Å}^{-1}$ (at large angle χ) while δq_z ranged from 0.003 to 0.0156 $\mathrm{Å}^{-1}$. For the out-of-plane or 'rod-scan' measurements, $\delta q_\parallel$ ranged from 0.04 to 0.044 $\mathrm{Å}^{-1}$ while δq_z ranged from 0.008 to 0.022 $\mathrm{Å}^{-1}$.

In addition, the average domain size L_D of the monolayers can be determined from the width of the Bragg peak. After taking the instrumental broadening into account, the domain size L_D can be calculated from the observed width $\Delta q_\parallel$

$$L_\mathrm{D} = \frac{2\pi}{\Delta q_\parallel}. \tag{3}$$

Note that if other types of broadening exist, such as a variation of the intermolecular distance [11], these factors must be corrected for. We note that the area under the Bragg peaks, i.e. the integrated intensity, gives a measure of the number of molecules that assemble in an ordered fashion. Furthermore, structural information along the surface normal can be obtained by performing rod-scans that measure the intensity variation of a surface Bragg peak along $\boldsymbol{q}_z$. Assuming the molecules as rigid cylinders, the tilt structure of the monolayers can be estimated from the peak position q_z and the width of the peak Δq_z as [43]

$$|\boldsymbol{q}_z| = |\boldsymbol{q}_\parallel| \tan\theta_\mathrm{t} \cos\chi \tag{4}$$

$$\Delta q_z \approx \frac{2\pi}{D}, \tag{5}$$

where θ_t and χ are the tilt angle with respect to the surface normal and the tilt direction with respect to the direction of $\boldsymbol{q}_\parallel$ respectively. D is the thickness of the monolayer. Also, information on the thermal motion of the molecules can be retrieved from the temperature dependence of the diffraction intensity, which is known as the Debye–Waller effect. The attenuation of the intensity is proportional to $e^{-q^2\langle u^2\rangle}$, where $\langle u^2\rangle$ is the mean square displacement along the momentum transfer $\boldsymbol{q}$.

A rectangular coordinate system is used with unit vectors $\boldsymbol{a}$ and $\boldsymbol{b}$ equal to 4.997 Å and 8.66 Å. The reciprocal lattice vectors $\boldsymbol{a}^* = 1.257\ \mathrm{Å}^{-1}$ and $\boldsymbol{b}^* = 0.726\ \mathrm{Å}^{-1}$ are labeled as $(1, 0)$ and $(0, 1)$, respectively. The surface normal is defined as the $\langle 111\rangle$ direction of the face-centered cubic structure of gold. The third unit vector $\boldsymbol{c}$ corresponds to the Au (111) Bragg point and is equal to 2.356 Å ($\boldsymbol{c}^* = 2.667\ \mathrm{Å}^{-1}$). The hexagonal peaks of a $(\sqrt{3}\times\sqrt{3})\mathrm{R}30^\circ$ structure appear, in this rectangular coordinate system, at the $(1, 1)$ position and at five other symmetry-equivalent positions: $(1, -1)$, $(-1, 1)$, $(-1, -1)$, $(0, 2)$, and $(0, -2)$.

2.3. LEAD

The LEAD studies were performed in a bolometric-detection-based atom diffractometer that allows an in situ sample preparation. The diffractometer has been described in detail elsewhere [44–48]. A monoenergetic beam of helium (wavevector $\boldsymbol{k}_i = 5.33\ \text{Å}^{-1}$ and $d\boldsymbol{k}_i/\boldsymbol{k}_i \approx 2\%$) produced by supersonic expansion is made to impinge on the surface at fixed incident angle θ_i about 60° from the surface normal. The angular distribution of the scattered helium intensity is measured by the detector for different values of θ_f with the substrate temperature held at 40 K. An 'in-plane' scattering configuration was used, i.e. the incident beam, the surface normal $\boldsymbol{n}$, and the detector were all in the same horizontal plane. Thus, the parallel momentum transfer $\boldsymbol{q}_\parallel$ can be determined by

$$|\boldsymbol{q}_\parallel| = |\boldsymbol{k}_i|\,(\sin\theta_f - \sin\theta_i). \quad (6)$$

The resolution was determined by the size of the detector. For the present studies, the $\boldsymbol{q}_\parallel$ resolution is $\sim 0.06\ \text{Å}^{-1}$, whereas the azimuthal resolution is only $\sim 1\ \text{Å}^{-1}$ due to the vertical slit collimated beam geometry used to increase detection sensitivity.

3. Structural data

3.1. Striped phase

Fig. 2a shows the observed two-dimensional reciprocal space map of the striped phase of MMB monolayers at a q_z of $0.4\ \text{Å}^{-1}$. In the coordinate system used here, the surface mesh of the striped phase is identified by two vectors $\boldsymbol{u}^*$ and $\boldsymbol{v}^*$ at $(0, 0.375)$ with $q_\parallel = 0.272\ \text{Å}^{-1}$ and at $(0.5, 0)$ with $q_\parallel = 0.6285\ \text{Å}^{-1}$. This corresponds to real-space periodicities of 23.08 Å and 10 Å, respectively. With respect to the substrate surface mesh, the overlayer can be accurately described as a rectangular $(8 \times 2\sqrt{3})$ net. It is important to note that systematic absences along both h and k axes and intensity modulation of the peaks of $h = 0.5a^*$ were observed in the diffraction pattern. Their implications will be discussed later. The symbol '×' indicates that this particular reciprocal spot was scanned and that the measured intensity was found to be at the noise level. Fig. 2b shows a radial scan through the $(0.5, 0.375)$ Bragg peak. Assuming a linear back-

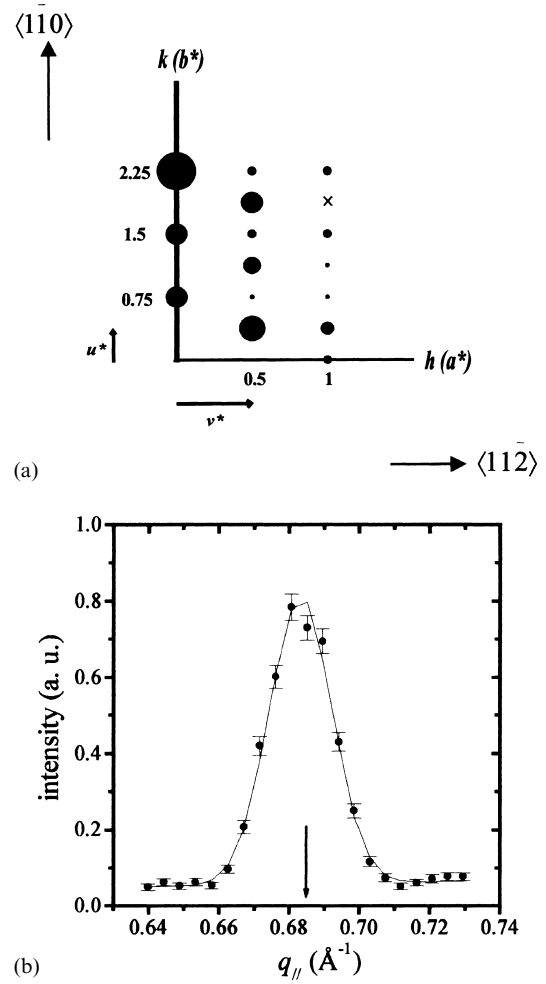

Fig. 2. (a) Observed reciprocal space map for the striped phase of MMB monolayers at $q_z = 0.4\ \text{Å}^{-1}$. With the rectangular coordinate system used, the vectors $\boldsymbol{u}^*$ and $\boldsymbol{v}^*$ are at $(0, 0.375)$ and $(0.5, 0)$, corresponding to lattice spacings of 23.08 Å and 10 Å respectively. Note that there are systematic absences along the h and k axes. The radii of the circles have been scaled to the normalized integrated intensities. The measured intensity at the peak $(1, 1.875)$ was at the noise level. (b) Data (solid circles) and Gaussian fit (solid line) to the radial scan through the $(0.5, 0.375)$ Bragg peak show that the structure of the striped phase can be described by a commensurate rectangular $(8 \times 2\sqrt{3})$ surface lattice. The expected peak position for the commensurate lattice is indicated by a vertical arrow.

ground and a Gaussian peak shape, a least squares fit (the solid line) to the data (the solid circles) gives a peak at $q_{\parallel}=0.6830\pm0.0006$ Å^{-1}. The error bar was taken as three times the standard deviation of the fit. Similar scans of all peaks indicated in Fig. 2a were taken to obtain the two-dimensional diffraction pattern.

The molecular fragment length or, to be precise, the distance between the S atom and the methyl C atom, is calculated to be 10.376 Å. The length of the molecular fragment is derived using the bond lengths taken from the crystallographic data of 4,4′-biphenyldithiol [49] and *p*,*p*′-bitolyl ($CH_3-C_6H_4-C_6H_4-CH_3$) [50]. The long axis of the unit mesh (23.08 Å) is close to twice this length. Assuming that the S—H bonds break in the assembly process, the measured dimension suggests that along the $\langle 1\bar{1}0\rangle$ direction (nearest-neighbor direction of the substrate) the molecular fragments are arranged in 'stripes' and have a 'head-to-head' orientation. However, given that the van der Waals radii of methyl groups are approximately 1.75–2.0 Å (as in the case of methane dimers, 2 Å corresponds to the radius of the methane molecule at the potential minimum and 1.75 Å corresponds to the radius at the zero interaction energy point [51,52]), and the S—S distance is at least 2.1 Å [53], the dimension of the unit mesh is about 3 Å too short for the molecular fragments to be lying flat on the surface with their axes parallel to the $\langle 1\bar{1}0\rangle$ direction. This suggests that the fragments are either tilted from the surface and/or aligned off the $\langle 1\bar{1}0\rangle$ direction.

The systematic absences in the diffraction pattern mentioned above provide crucial information as the presence of an underlying symmetry in the structure becomes evident. For all the Bragg peaks of the striped phase, the parallel momentum transfer $\boldsymbol{q}_{\parallel}$ can be written as $m\boldsymbol{u}^*+n\boldsymbol{v}^*$, where m and n are integers (see Fig. 2a). The diffraction pattern shows that when m is odd and n is zero, the Bragg peaks are absent. The same phenomenon is observed when n is odd and m is zero. These systematic absences imply two possible symmetries, namely the presence of a glide plane along the $\langle 1\bar{1}0\rangle$ direction or a centered rectangular unit mesh, which would lead to the situation where the Bragg peaks with an odd $(m+n)$ value would *also* be forbidden (which is not the case).

Fig. 2a also shows that there is an intensity modulation of the Bragg peaks. When $n=1$ (i.e. $h=0.5a^*$, note that the units of the h and k axes are respectively a^* and b^*), the peaks with an even m value are weaker than the peaks with an odd m value, i.e. the peaks with an odd $(m+n)$ value are weaker than the peaks with an even $(m+n)$ value. This trend is also qualitatively exhibited in the peaks when $n=2$ (i.e. $h=a^*$). This observation indicates that the unit mesh is likely to have a centered rectangular symmetry with some distortion, which, with the data available at present, is difficult to quantify.

With the findings described above, possible structures of the striped phase of MMB monolayers can be hypothesized. As the data suggest that the symmetry of the structure is close to centered rectangular, the proposed structure has a centered rectangular symmetry. Fig. 3 is the projection of the proposed structure looking down the surface normal. Molecular fragments #1 and #2 are oriented 'head-to-tail' and are rotated from the long axis of the unit mesh by 15°. In the model, the S—S spacing is ~2.2 Å and the C—S—S angles are 103° as in the case of dialkyl disulfides [53]. From consideration of the required spacing between the methyl groups (≥3.5 Å) and the van der Waals dimensions of the phenyl rings (the ring diameter is 6.4 Å and the width is 3.3 Å), both fragments #1 and #2 are suggested to tilt at least ~15° from the surface with their S headgroups anchoring on the surface. In this model, the spacings between the methyl groups can become as large as 4 Å [51,52]. Note that recent X-ray standing wave data [54,55] have established that the equilibrium disulfide unit in SAMs of *n*-decanethiol on Au(111) has the S atoms at a different height from the surface. It is possible that a similar situation could be present in the case of the MMB monolayers discussed here. If this is the case, the two MMB fragments belonging to the same dimer may be tilted differently from the surface.

One more structural parameter in the striped phase needs to be addressed, i.e. the dihedral angle ψ about the inter-ring C—C bond of the biphenyl units (see Fig. 4). For a biphenyl molecule, the

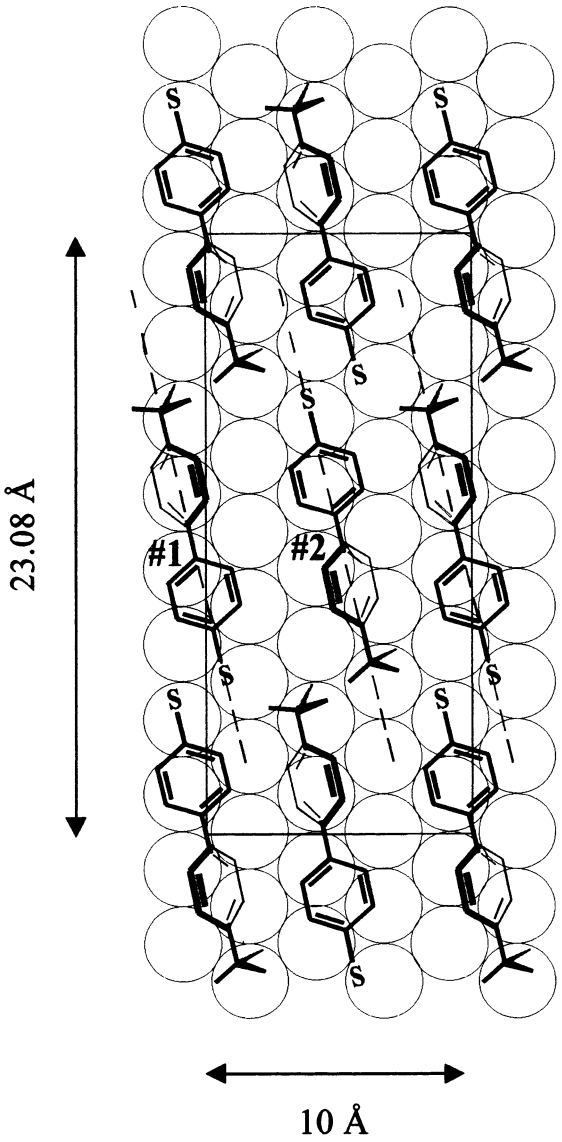

Fig. 3. Proposed structure for the striped phase of MMB monolayers. A projection of the structure looking down the surface normal is shown (drawn to scale). The open circles represent Au atoms. The rectangle outlines the observed unit mesh. As explained in the text, the systematic absences and the intensity modulation imply a centered rectangular symmetry with some distortion. Along the long axis of the unit mesh, molecular fragments are likely to orient 'head-to-head'.

dihedral angle ψ is known to be very responsive to its environment because of a relatively small energy barrier for rotation (6 kJ/mol) [56–58].

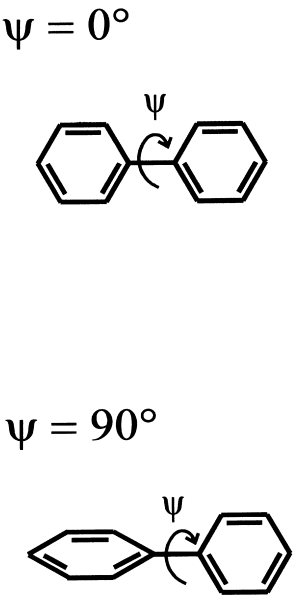

Fig. 4. The dihedral angle ψ of a biphenyl molecule.

Therefore, given the strong molecule–surface and molecule–molecule interaction, it is reasonable to assume that the dihedral angle rotation can be of help in achieving a minimum packing energy in the proposed structure.

To summarize, the diffraction pattern of the striped phase of MMB monolayers is consistent with a distorted rectangular lattice in which molecules in the same row are arranged head-to-head while molecules in adjacent rows are arranged head-to-tail. A possible structure suggests that the molecular axes are close to but inclined with respect to the surface and that the biphenyl units are rotated about the molecular axes. The proposed structure for the striped phase implies a packing density of 57.7 $Å^2$ per fragment. However, we stress that the proposed structure is tentative and that it may have to be revised as more data of a different nature (for instance from the X-ray standing wave technique [54,55]) become available to complement the present study.

3.2. Hexagonal phase

3.2.1. In-plane X-ray diffraction

As will be discussed further in Section 5, another phase was observed. The diffraction peaks

observed for the monolayer (solid circles) and the substrate surface mesh (hatched circles) are shown in Fig. 5a. Only the (1, 1) Bragg peak and its symmetry equivalent peaks could be detected for the monolayers. Fig. 5b shows a radial scan through one of these peaks. Assuming a linear background and a Gaussian peak shape, a least squares fit (solid line) to the data (solid circles) gives a peak at $q_{\parallel} = 1.454 \pm 0.001$ Å^{-1}, which corresponds to a periodicity of 4.321 ± 0.003 Å in real space, which, in turn, is within 0.12% of the periodicity along the $\langle 1\bar{1}0 \rangle$ direction expected from a $(\sqrt{3} \times \sqrt{3})$R30° surface lattice. The absence of other Bragg peaks in the spots indicated by '×' symbols is consistent with a purely hexagonal $(\sqrt{3} \times \sqrt{3})$R30° lattice. Although we will discuss the possible existence of a superlattice later (see Sections 3.2.2 and 6), we denote this phase as the hexagonal phase.

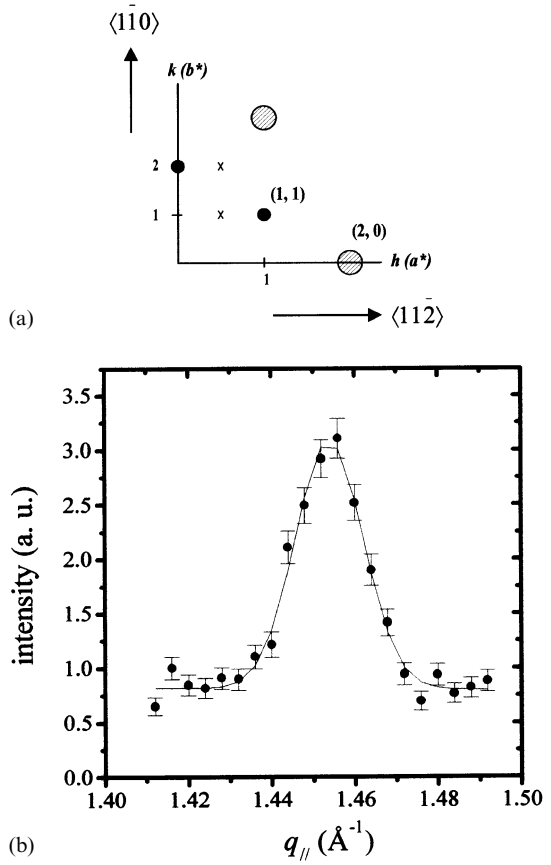

Fig. 5. (a) Observed reciprocal-space representation of the hexagonal phase of MMB monolayers (solid circles) and Au(111) surface lattice (hatched circles) at $q_z = 0.4$ Å^{-1}. The Bragg peak of the monolayers and that of the substrate are indexed as (1, 1) and (2, 0) respectively. The '×' symbols mark the points in the reciprocal space where no diffraction was observed. The diffraction pattern shows that the structure of the hexagonal phase can be described by a simple $(\sqrt{3} \times \sqrt{3})$R30° lattice. (b) Radial scan (solid circles) and the Gaussian fit (solid line) through the (1, 1) Bragg peak.

It is worthwhile to compare this diffraction pattern with the high coverage phase of C_n. The '×' symbols mark the points in reciprocal space where diffraction is expected from the $c(4\sqrt{3} \times 2\sqrt{3})$R30° structure as observed in C_n. For the hexagonal phase of MMB monolayers, no diffraction was observed at these positions. As it has been shown that the superlattice features in C_n are due to dimerization of the S atoms at the S–Au interface [8,54,55,59], the absence of these peaks for MMB monolayers suggests that in the hexagonal phase, the S headgroups pack in the same way as the molecular backbones. This would imply that the thiol molecules assemble as thiolates.

3.2.2. LEAD

Fig. 6 shows a LEAD scan taken at 40 K in the $\langle 1\bar{1}0 \rangle$ direction from the hexagonal phase of MMB/Au(111). Fig. 7 displays instead a series of diffraction scans taken at several azimuthal angles separated by 5° intervals. The characteristic peaks (marked by solid lines) of the simple hexagonal $(\sqrt{3} \times \sqrt{3})$R30° mesh are clearly visible. A small peak at $q_{\parallel}$ around -0.5 Å^{-1} is also visible in the $\langle 1\bar{1}0 \rangle$ scan, which indicates a possible tripling of the basic hexagonal mesh. The expected position is at -0.484 Å^{-1} (marked by the dashed line). The specular peaks shown in Figs. 6 and 7 have an average width of 1.31°. Correcting for the apparatus resolution width of 1.01 ± 0.09° yields a domain-size-determined peak width of 0.82 ± 0.11° corresponding to an average domain size of 175 ± 25 Å. The lack of a pedestal in the specular peak indicates a very stiff layer with little inelastic scattering (see below).

Fig. 8 displays the diffraction peak widths (determined from the widths of the diffraction

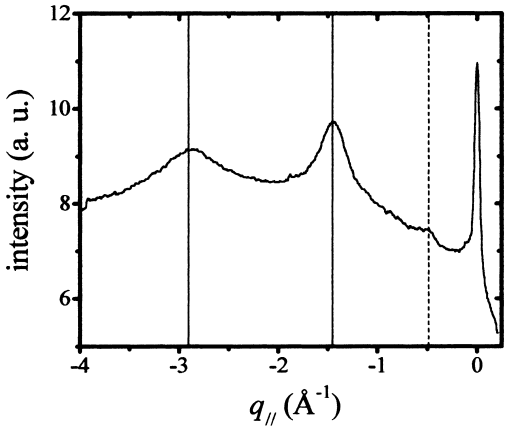

Fig. 6. LEAD pattern from the surface of the hexagonal phase of an MMB monolayer taken in the $\langle 1\bar{1}0\rangle$ direction at 40 K. Eight scans have been added together to increase the signal-to-noise ratio. The vertical solid lines indicate the expected positions of the first- and second-order diffraction peaks for a $(\sqrt{3}\times\sqrt{3})$R30° mesh. The vertical dashed line indicates the peak position expected for a superlattice with a threefold larger periodicity.

peaks corrected for apparatus resolution) as a function of $q_{\|}$ for eight different scans along the $\langle 1\bar{1}0\rangle$ direction. The large peak widths cannot simply be due to a small domain size because the widths of the first- and second-order peaks are very different. The increase in peak width for the higher-order diffraction peaks could be a result of either crystal imperfections (see below) or a strongly inhomogeneous velocity distribution in the He beam (which we know to be very narrow).

A lattice disorder of the first type [60] results when each domain has a well-defined periodicity but different domains have slightly different lattice parameters. The resulting diffraction peaks are the sum of the peaks produced by all the domains with slightly different lattice constants. The linear fit of the data (filled circles) in Fig. 8 indicates a domain size of 135 ± 65 Å (as indicated by the y-intercept), and the width of the lattice spacing distribution is $\sim$18% (as indicated by the slope) about the thiol–thiol distance of 5 Å. The data fit well to a straight line, indicating a lattice disorder of the first type. It is important to note that the X-ray measurements do not show the presence of this type of imperfection, which could be due to the S atoms (which anchor at the interface) being

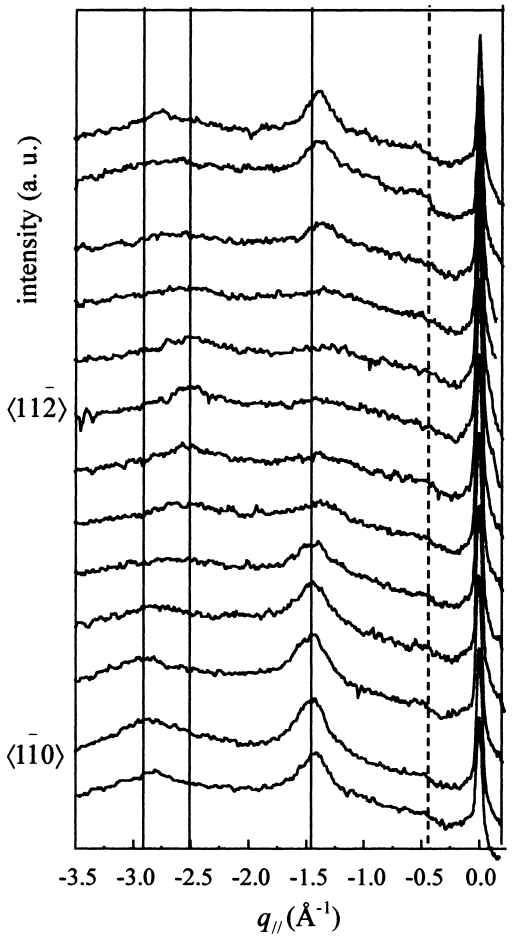

Fig. 7. LEAD scans of MMB on Au(111) at 40 K at different azimuthal angles of 5° apart. The vertical lines mark the positions of the diffraction peaks expected for a $(\sqrt{3}\times\sqrt{3})$R30° mesh: first-order ($q_{\|}=-1.45$ Å^{-1}) and second-order ($q_{\|}=-2.9$ Å^{-1}) along the $\langle 1\bar{1}0\rangle$ direction, and first-order ($q_{\|}=-2.51$ Å^{-1}) along the $\langle 11\bar{2}\rangle$ direction. The position of a possible superlattice peak at $q_{\|}=-0.484$ Å^{-1} is marked with a dashed line.

ordered while the top of the molecules could be slightly displaced from their $(\sqrt{3}\times\sqrt{3})$R30° positions.

A top surface disorder may be caused by a mismatch between the lowest energy configuration of the molecular backbone of MMB and that of the underlying $(\sqrt{3}\times\sqrt{3})$R30° structure of the S headgroups. Biphenyl has been found to have an 8.04 Å × 5.51 Å rectangular crystal structure [56,61], whereas the $(\sqrt{3}\times\sqrt{3})$R30° structure of

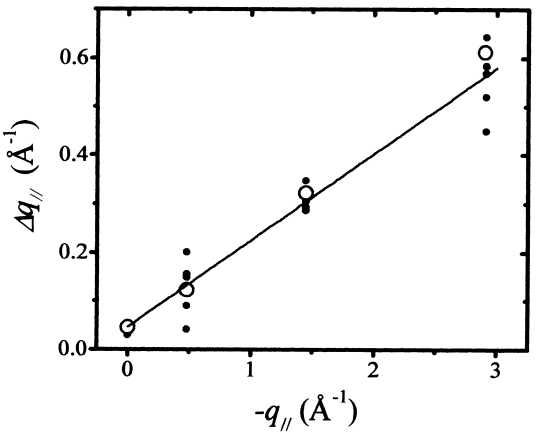

Fig. 8. Diffraction peak width as a function of $q_{\parallel}$ taken from eight diffraction scans along the $\langle 1\bar{1}0\rangle$ direction (filled circles) are fitted by a straight line. Peak widths taken from the sum of the eight diffraction scans (Fig. 6) are also shown as open circles. The linear peak width dependence on $q_{\parallel}$ indicates the presence of lattice disorder of the first type [60].

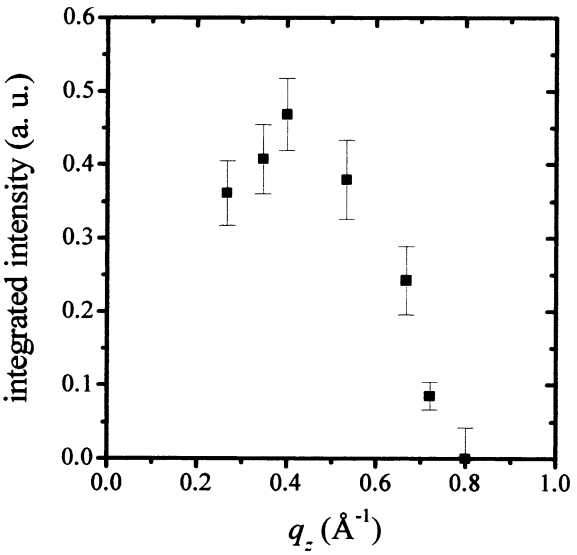

Fig. 9. Rod-scan data of the (1, 1) Bragg peak of the hexagonal phase. The intensity profile as a function of q_z suggests a tilt angle of MMB molecular backbone of no more than 19° with respect to the surface normal.

the S headgroups is equivalent to a centered rectangular mesh of 8.65 Å × 5.00 Å. Therefore, the molecular area of MMB monolayers will be ~2.5% larger than the $(\sqrt{3}\times\sqrt{3})$R30° mesh if the monolayer structure is determined more by the molecular backbone. MMB molecules may try to accommodate the strain by distorting from the vertical orientation leaving the S atoms in their $(\sqrt{3}\times\sqrt{3})$R30° positions (which would explain why this disorder was not observed in the GIXD studies) but producing the top surface disorder detected by the atomic beam diffraction, which is only sensitive to the position of the topmost layer of atoms.

3.2.3. *Out-of-plane X-ray scattering*

Fig. 9 shows a rod-scan of the (1, 1) Bragg peak in the limited q_z range from 0.2 to 0.8 Å^{-1}. From the q_z position and the width of the peak in the rod-scan, the tilt structure of MMB monolayers can be derived. The intensity profile is clearly not flat and the intensity steeply decreases as q_z increases above 0.4 Å^{-1}, which is strongly suggestive of a small but non-zero tilt angle. Given that measurements are available for only one Bragg rod, the tilt angle θ_t and the tilt direction χ cannot be unambiguously determined from the data [see Eq. (4)]. By considering tilt directions either along the nearest neighbors ($\chi=0°$) or along the next-nearest neighbors ($\chi=30°$), a probable tilt angle (with respect to the surface normal) can be estimated. The maximum of the profile is at most at $q_z=0.4$ Å^{-1}, considering that the data points at very small q_z are generally more difficult to measure. With the maximum at $q_z\leq 0.4$ Å^{-1} the tilt angle $\theta_t\leq 15.4°$ for $\chi=0°$, whereas the tilt angle $\theta_t\leq 17.6°$ if $\chi=30°$. Taking into account all possible errors we can say that θ_t for MMB molecules is not more than 19°, which is much less than for the hydrocarbon chains of thiols in C_n that are tilted by more than 30° [28].

In summary, in the hexagonal phase, MMB molecules are almost vertical and pack hexagonally. As GIXD is not very sensitive to the relative positions of the phenyl rings of the biphenyl units, the dihedral angle ψ in the hexagonal phase cannot be determined from the data available at present. From the unit mesh dimensions of the hexagonal phase, the area per molecule is 21.6 Å^2. Thus the density of the hexagonal phase is 2.7 times larger than that of the striped phase.

Although 'pure' striped samples could be pre-

pared, the hexagonal phase was found to coexist with the striped phase in some samples (see Section 5). The samples examined by LEAD might not have a complete coverage of the hexagonal phase. Note that the structural findings, however, are not invalidated by the co-existence of phases because the striped phase does not contribute to the intensity at the (1, 1) Bragg peak.

4. Thermal behavior

4.1. Striped phase

In addition to the structure, the thermal behavior of the striped phase was examined by measuring the (0, 1.5) Bragg peak as a function of the substrate temperature. In order to study the intrinsic behavior of the striped phase, samples were annealed to 443 K before conducting the melting experiment. This was done because annealing under vacuum can remove the defects that may be present due to non-equilibrium growth effects. Also, as will be explained in Section 5, coexistence of the hexagonal phase and the striped phase was observed in some samples. After the samples were heated to $\sim$413 K, the hexagonal phase irreversibly disappears and only the striped phase is observed. Prior to each measurement, samples were held at the chosen temperature for 5 min to ensure thermal equilibrium.

Fig. 10 shows a series of radial scans through the (0, 1.5) Bragg peak at different temperatures. The scans were fitted with a Gaussian peak shape and a linear background and the peak positions at 289 ± 2 and at 437 ± 10 K are marked by solid lines in Fig. 10. The peak position is found to change from 1.088 ± 0.001 Å^{-1} at 289 K to 1.084 ± 0.001 Å^{-1} at 437 K. The peak positions correspond to unit mesh dimensions of 23.10 ± 0.01 Å and 23.18 ± 0.01 Å respectively. The expansion of the monolayer (which is 0.3%) is $\sim$14 times larger the expansion of the Au bulk lattice [53], implying that the monolayers cannot be commensurate over the entire temperature range.

In Fig. 11, the integrated intensity of the (0, 1.5) Bragg peak (at $q_z=0.4$ Å^{-1}) at different stages of

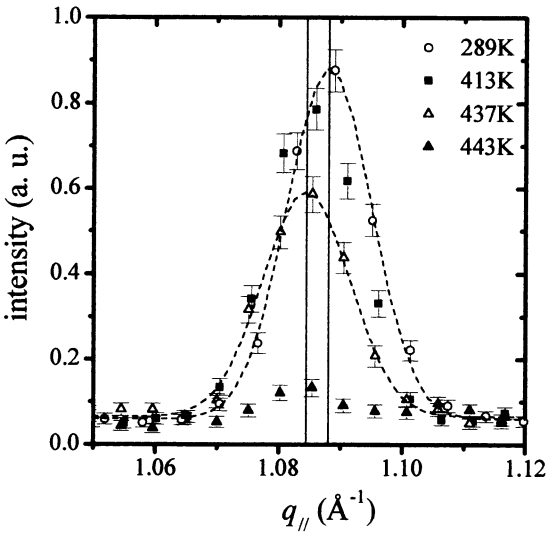

Fig. 10. Temperature dependence of the structure of the striped phase measured by radial scans through the (0, 1.5) Bragg peak at different temperatures. The symbols for each temperature are indicated in the figure. The dashed lines are the Gaussian fit to the data. As indicated by the solid lines, the unit mesh dimension changes by $\sim$0.08 Å when the sample is heated to $\sim$437 K.

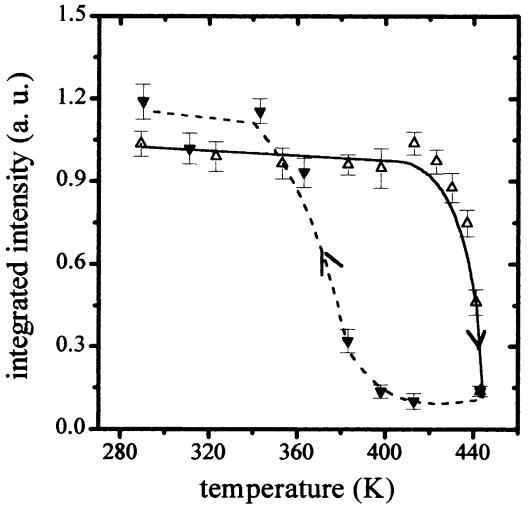

Fig. 11. The integrated intensity of the (0, 1.5) Bragg peak of the striped phase is plotted as the sample is heated (△) and cooled (▼). The arrows indicate the temperature cycling sequence. Note that the integrated intensity does not decrease after the thermal cycle is completed, which suggests the presence of a melting transition at $\sim$440 K. The presence of hysteresis is also evident.

the temperature cycle is plotted. Since upon cooling to room temperature the integrated intensity is found to be no less than what it was before the thermal cycling experiment, the drastic drop in the integrated intensity above 423 K is indicative of a melting transition. The small increment actually found ($\sim$15%) in the integrated intensity may be due to the elimination of a small fraction of a disordered phase that was present before the experiment. Note that hysteresis was observed, which typically is suggestive of a first-order transition. Furthermore, we found that neither the domain size nor the integrated intensity changes appreciably up to 423 ± 5 K, where the melting transition sets in. The second piece of information suggests that the Debye–Waller factor of the striped phase is very small.

The melting transition is almost complete at 443 ± 5 K. As estimated from the change in the integrated intensity, 87 ± 2% of the striped phase has melted after the monolayer was kept at 443 K for 2 min. If samples were held at this temperature for longer times (as was the case before melting), significant desorption was observed. The observations suggest that desorption takes place soon after the melting has completed. Such a high melting temperature can be attributed to the fact that the biphenyl units are rigid and, therefore, the molecules have less conformational freedom. To conclude, the results show that the striped phase is thermally quite resilient.

4.2. Hexagonal phase

The temperature dependence of the structure of the hexagonal phase was studied next. In Fig. 12, radial scans through the (1, 1) Bragg peak at 299 ± 1 K (■) and at 373 ± 3 K (□) are plotted. By fitting the scans with a Gaussian peak shape and a linear background, the peak positions, marked by solid lines in Fig. 12, were determined. The peak position was found to change from 1.451 ± 0.001 Å^{-1} at 299 K to 1.448 ± 0.001 Å^{-1} at 373 K. The shift in the position implies that an increase of the unit mesh dimension of $\sim$0.2% occurs. As the errors are relatively large, no definitive conclusions on the change in the unit mesh dimensions shall be drawn. In order to understand

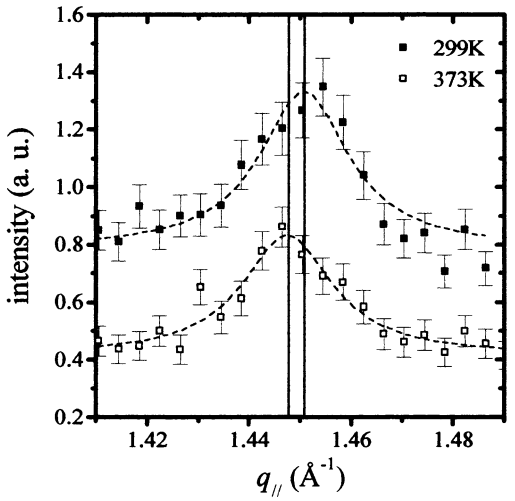

Fig. 12. Temperature dependence of the surface structure of the hexagonal phase as measured by GIXD. Radial scans through the (1, 1) Bragg peak at 299 K (■) and at 373 K (□) are plotted. The data at 299 K were translated vertically for viewing convenience. The dashed lines are the Gaussian fit to the data and the solid lines mark the peak positions of the fit. Owing to large uncertainty of the fit, changes in the unit mesh dimension cannot be determined from the data.

if the molecules tilt differently at different temperatures, rod-scans through the (1, 1) Bragg peak were performed at two different temperatures. The intensity profiles at 299 K (■) and at 376 K (○) are as shown in Fig. 13. The shapes of these rod-scans are very similar. This indicates that the tilt structure does not change significantly in this temperature range.

The thermal response of the hexagonal phase was also studied at higher temperature. Each measurement was taken after the sample was annealed at the target temperature for $\sim$7 min. Up to 393 K, the integrated intensity undergoes very little change. After annealing to $\sim$415 K for $\sim$7 min, the integrated intensity dropped to the noise level. From previous studies on the thermal behavior of C_n [62], we know that this property is a strong function of coverage. From the behavior of the hexagonal phase, we can infer that complete coverage by the hexagonal phase was never achieved in our experiments.

Fig. 14 shows LEAD spectra of the hexagonal phase taken at several different substrate temper-

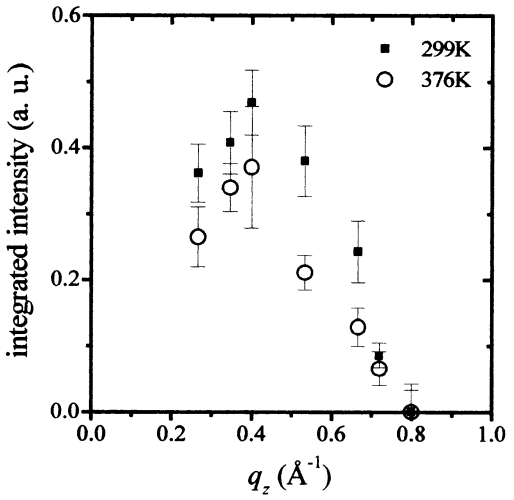

Fig. 13. Rod-scan of the (1, 1) Bragg peak of the hexagonal phase as a function of substrate temperature. The rod-scan data at 299 K (■) and at 376 K (○) are shown. No evidence of change in the tilt structure can be derived from these data.

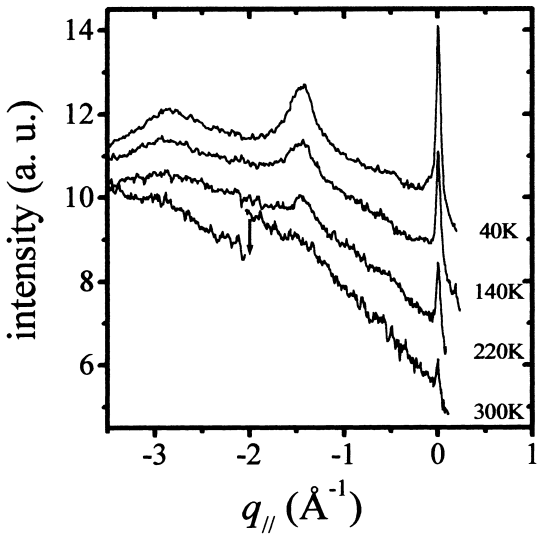

Fig. 14. Temperature dependence of LEAD patterns for the hexagonal phase of MMB monolayers.

atures. The MMB monolayer surface proves to be thermally more stable than any other organic surfaces we have studied thus far, as is evidenced by a visible specular peak even at room temperature. The integrated intensity of the specular peak can be used to determine $d\langle u_z^2\rangle/dT$, the rate of increase of the mean square of the vertical displacement $\langle u_z^2\rangle$ of the organic surface with respect to substrate temperature T. Table 1 compares the measurement of $d\langle u_z^2\rangle/dT$ for the MMB surface with those of the hexagonal phase of C_{10}, the lying-down striped phase of C_{11}, and a bare gold substrate. One sees that the hexagonal phase of the MMB monolayers is a stiffer surface than all other surfaces except that of the bare gold itself.

Table 1
Debye–Waller factors derived from specular peak attenuation for various surfaces

Surface	$d\langle u_z^2\rangle/dT$ (Å^2/K)
Bare Au(111)[a]	$(0.32\pm0.03)\times10^{-4}$
Hexagonal phase of MMB monolayers	$(0.6\pm0.05)\times10^{-4}$
Striped phase of C_{11}[b]	$(1.25\pm0.03)\times10^{-4}$
Hexagonal phase of C_{10}[c]	$(2.2\pm0.1)\times10^{-4}$

[a] Ref. [63].
[b] Ref. [48].
[c] Ref. [64].

Vertical motion of individual MMB molecules would require both compression and relative motion of the phenyl groups. The stronger π–π interaction between the phenyl groups and the rigidity of the phenyl group itself make the MMB monolayers a more rigid body than that of the interdigitated alkyl chains. In addition, the lack of conformational freedom imposed by the near-vertical molecular orientation mentioned above provides another barrier to molecular movement. Finally, above the rather rigid molecular base, only the vibrations of the terminal C—C bond and the methyl C—H bonds can result in a vertical displacement of the terminal methyl groups. The methyl group in C_n, however, can undergo a vertical displacement through 'softer' stretching and bending vibrations of C—C bonds allowed by the zigzag backbone of aliphatic thiol molecules.

5. Influence of growth conditions on structure and quality of the monolayers

The ways in which different preparation techniques and conditions determine the occurrence of the various phases and their structural coherence

were investigated. The preparation techniques employed were (see details below): (i) conventional liquid-phase (solution) deposition; (ii) in vacuo vapor-phase deposition; and (iii) 'alkane-assisted' growth mode.

After conventional liquid-phase deposition, no phase other than the hexagonal phase was seen. However, in only one out of the five solution-grown samples, the hexagonal phase was observed. The structural quality was rather poor and the domain size was only ~ 65 Å. For the other four samples, no diffraction features were found. This implies that in these four samples either the hexagonal phase does not exist or the domain size is smaller than the detection limit. Also, ten other solution-grown films were independently characterized either by LEAD or by STM. The STM measurements were performed in the laboratories of Professor A. Kahn at Princeton University and Dr G. Poirier at the National Institute of Standards and Technology. The hexagonal phase was observed in only one of the ten films. There was no evidence of ordered phases in the remaining nine films. Thus, the observations indicate that the hexagonal phase is difficult to form, at least from solution. Relating to this, there are two reports on the characterization of solution-grown monolayers of 4-mercaptobiphenyl on gold, a system very similar to MMB monolayers. While one report found no evidence of ordered structure [24], the other report suggested that the compound formed an ordered monolayer [25] but offered no structural evidence.

In vacuo vapor-phase deposition was tried next. Notice that besides the cleanliness and control over the growth conditions, vapor-phase deposition has the advantage of making direct and in situ studies of the growth possible without the necessity for a special in situ liquid-phase X-ray scattering cell [30]. As might be expected, the low-density striped phase was found in the initial stage of the growth as in the case of the C_n [30]. The domain size of the films was found to vary considerably with the substrate temperature. For films grown at 289 K the domain size was found to be ~ 180 Å, whereas for films grown at 387 K the domain size was found to be substrate-limited, i.e. domain sizes well above 1000 Å. Furthermore, high-quality striped phase with large domain sizes could easily be prepared by annealing the films prepared at the lower temperature. A striped phase covering the entire surface was found in essentially all growth experiments that have been attempted, irrespective of the growth conditions.

In the in vacuo growth experiments, only at relatively low substrate temperatures (283 K) indications of another structure were found. These came from diffraction peaks corresponding to a lattice spacing of 3.4 Å (data not shown). Considering the van der Waals dimensions of the benzene rings (6.4 Å × 3.3 Å), the observed spacing hints at a structure comprised of molecules with the biphenyl units stacking in parallel. However, this structure was obviously unstable and disappeared upon further deposition (with growth of the striped phase), so it will not be discussed further.

According to Ref. [30], the best chance to prepare a standing-up structure for the alkanethiols appears to be at low substrate temperatures (<293 K), long exposure times (several hours), and at higher incident flux [which is achievable here by heating the source to an elevated temperature (>323 K)]. Under these conditions and subsequent annealing, the hexagonal phase was observed. However, even when the hexagonal phase was obtained, the small integrated intensity indicated that it did not correspond to a full coverage monolayer, and coexistence of the hexagonal and the striped phases was observed. This shows that the striped phase apparently forms an effective 'kinetic trap' and prevents the growth of the high-density hexagonal phase.

As an alternative to conventional vapor-phase deposition, and as a step towards liquid phase growth, 'alkane-assisted' growth was employed. In this methodology, which has been successfully applied to control the growth kinetics of C_{10} [41], a layer of alkane (*n*-dodecane or *n*-octadecane) is deposited followed by deposition of the thiols. The idea is to modify the adsorption energetics such that, under certain conditions, the evolution of the striped phase can be disturbed and the growth of the high-density hexagonal phase is, perhaps, facilitated.

In the first experiment with the alkane-assisted

growth, there were indications that the kinetics of the self-assembly were modified. The striped phase was seen in the beginning. Later, the hexagonal phase was observed concomitant with the disappearance of striped phase. Seven more films were then prepared by using alkanes of two different chain lengths and by co-depositing alkane with the thiol. In only one of the seven films was the hexagonal phase observed, but it disappeared in a very short time. Therefore, we have no proof that pre-adsorption of alkane is effective in promoting the formation of the hexagonal phase. However, as the search in parameter space was quite limited it is possible that this growth method can control monolayer growth kinetics and phase formation during in vacuo deposition.

6. Discussion

6.1. Structure

The striped phase found for MMB monolayers is quite similar to that which is obtained for C_n [33,65]. The main difference is the doubling of the periodicity of the monolayers in the direction perpendicular to the molecular axes. Note that an oblique $(p \times \sqrt{3})$ lattice and a lamellar structure have been observed respectively in the monolayers of *n*-alkane on Pt(111) [66] and on Au(111) [67], in which the adsorbates are also believed to lie flat on the surface with the alkyl chains fully extended.

The doubling of the short lattice spacing of the unit mesh of MMB monolayers can be explained by the constraints provided by the biphenyl units. As the transverse size of alkyl chains in the bulk is $\sim$4.5 Å [61], the hydrocarbon backbone of the adsorbates in both alkane on Pt and on Au systems can fit nicely into the $\sqrt{3}$-spacing, which is 4.8 Å in the case of Pt(111) and 4.995 Å in the case of Au(111). Since the phenyl units of MMB molecules have transverse van der Waals sizes that differ substantially in the *x* and *y* directions (3.3 Å versus 6.4 Å, assuming that the *z* direction is that of the molecular backbone), the molecules could adapt themselves to a $\sqrt{3}$-periodicity only if the benzene rings were tilted with respect to the substrate and the dihedral angles would all be near 0°. Assuming that adjacent molecules orient 'head-to-tail' (see fragments #1 and #2 in Fig. 3), doubling the periodicity can keep the molecular density essentially unchanged and minimize the dihedral strain.

The molecular structure also affects the packing of the high-density hexagonal phase observed in both systems. The structure of the hexagonal phase of MMB monolayers is consistent with a commensurate $(\sqrt{3} \times \sqrt{3})R30°$ lattice, whereas the structure of C_{10} can be described by a $c(4\sqrt{3} \times 2\sqrt{3})R30°$ lattice, in other words, a $c(4 \times 2)$ superlattice of the simple commensurate $(\sqrt{3} \times \sqrt{3})R30°$ lattice [34,62,68–71]. For C_n, a recent high-resolution electron energy loss spectroscopy study [59] and X-ray standing wave measurements [54,55] have shown the presence of S dimers at the S–Au interface, which implies the existence of at least a gauche defect at the C atom located next to the S atom [8]. The fact that the $c(4 \times 2)$ superlattice is not observed in MMB monolayers can be attributed to the rigidity of the biphenyl units. Indeed it is not possible for two MMB molecules to be parallel and next to each other and still reduce the S—S spacing significantly.

As discussed earlier, the rod-scan data for the hexagonal phase of MMB monolayers show that the molecules tilt less than 19° from the surface normal. Previous GIXD studies of C_n found that for the hexagonal phase the tilt angle of the alkyl chains with respect to the surface normal ranged from 33° for $n=10$ to 31° for $n=30$ [28]. The smaller tilt angle for MMB reflects the fact that, in this system, the molecules do not need to tilt to maximize their van der Waals interactions when their spacing is constrained to be 5 Å, as a small adjustment of the dihedral angle is sufficient to do that. The area per molecule of the $(\sqrt{3} \times \sqrt{3})R30°$ lattice is 21.6 Å^2. For the C_n, the cross-sectional area of the bulk *n*-alkane is 18.6 Å^2 [61], leading to a predicted tilt angle of 31°. Considering the van der Waals dimensions of the phenyl rings (with a cross-sectional area of 21.1 Å^2), the 'predicted' tilt angle of the MMB molecules becomes approximately 12° [tilt angle $\sim \cos^{-1}(21.1/21.6)$].

The data reported here show that the molecular backbone can be used to change the structural details of both the striped phase and the hexagonal phase, the basic periodicity of the striped phase and the tilt angle in the close-packed 'standing-up' phase.

6.2. Thermal behavior

6.2.1. Striped phase

The higher thermal stability of MMB monolayers, which melt 60° higher than C_{10} (the data for C_{10} were taken from Ref. [5]), can be made plausible in terms of the energetics of the system that can be estimated from the physisorption enthalpies. From recent studies of the adsorption enthalpies for *n*-alkanethiol and *n*-alkane on gold, the physisorption enthalpy for an *n*-decyl chain, i.e. $CH_3-(CH_2)_9-$, is estimated to be ~71 kJ/mol [72,73]. These studies also reported that the physisorption enthalpy for benzene on gold is ~60 kJ/mol and that the contribution of a methyl group is ~16 kJ/mol. Assuming simple additivity, the physisorption enthalpy of 4-methylbiphenyl is estimated to be ~136 kJ/mol if the biphenyl units lie prone on the surface. Although the biphenyl units of the molecules do not lie flat on the surface as suggested in the model (see Fig. 3), the calculation offers a higher limit of the energetics of the molecule–substrate interaction. Taking into account that the lateral interactions are also larger in MMB monolayers compared with C_{10}, a 60°C difference in melting temperature is understandable. We noted in passing that in the bulk 4-methylbiphenyl melts about 80°C higher than *n*-decane. Clearly the sulfur–substrate interaction makes these two systems more similar to each other than the pure substances.

6.2.2. Hexagonal phase

Fig. 15 shows the integrated intensities of the (1, 1) peaks of MMB monolayers (■) and C_{10} (□) as a function of substrate temperature. The MMB monolayers remain crystalline up to at least 393 K, whereas full-coverage C_{10} almost completely melts at ~373 K. Before the melting transition takes place, the intensity for MMB monolayers is basically unchanged, whereas the intensity of C_{10} drops appreciably. This implies that the Debye–Waller factor of C_{10} is substantially larger than that of MMB monolayers, which can be attributed to the lack of conformational freedom of the biphenyl units. Despite the fact that the data for MMB were measured in a film that contained both the hexagonal and the striped phases, the data show that MMB monolayers are more robust than C_{10}, especially taking into account that a higher thermal stability in films of full coverage than in films of partial coverage is expected. Again, this is the result of multiple factors that include stronger molecule–molecule and molecule–substrate interactions. The key factor remaining, however, is the lack of backbone flexibility.

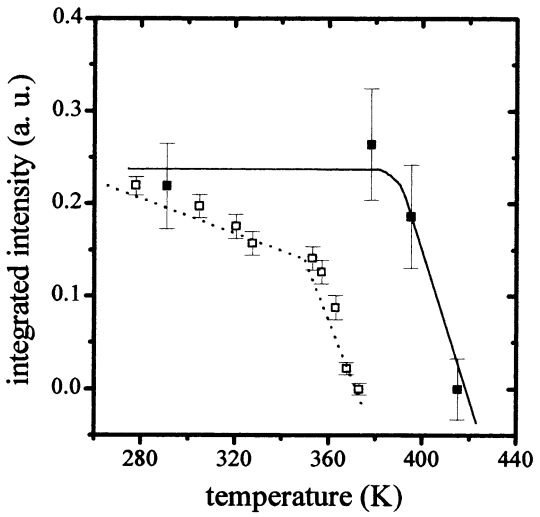

Fig. 15. Integrated intensities of the hexagonal phase of MMB monolayers (■) and C_{10} (□) as a function of temperature. Notice that the intensity of C_{10} at room temperature is scaled to that of MMB monolayers and that the relative intensity is not to be inferred from this plot. The solid and dotted lines are only guides to the eye.

6.3. Growth behavior

As outlined in Section 5, various growth techniques and conditions have been employed. The qualitative growth behavior of MMB monolayers is similar to that of C_{10}, in that the growth proceeds through a striped phase at low coverage and a hexagonal phase at higher coverage. However, the

different rigidity of the molecular backbone of MMB also introduces significant changes. The most important differences are the poor structural coherence of solution-grown films and the strong resistance against the formation of the hexagonal ('standing-up') phase. This is to say that the striped phase of MMB monolayers acts as a very effective 'kinetic trap' during the growth, whereas the poor structural integrity of solution-grown MMB monolayers is likely related to the limited mobility of the molecules during the growth.

The larger barrier between the striped phase and the hexagonal phase in MMB monolayers may be due to both the stronger molecule–substrate interaction and the rigidity of the molecules. It has been shown that, for molecules lying down, the molecule–substrate interaction of C_n becomes stronger as the alkyl chain becomes longer [72]. As a result, *n*-octadecanethiol has a comparable molecule–substrate interaction with that of MMB molecules. As high-quality hexagonal phases of C_{18} can be grown without any difficulty [74], we conclude that the conformational freedom of the backbone plays a more important role than the simple energetics of the interaction with the substrate.

A stronger molecule–substrate interaction and a rigid molecule also lead to a lower surface mobility of the molecules. Thus, the variability of the quality of striped phase of MMB monolayers with the growth conditions can be explained in terms of surface diffusion. Freshly prepared monolayers of the striped phase grown at room temperature are of poor quality. At a higher deposition temperature the surface diffusion increases, and as a result the domain size of the striped phase can be as large as the substrate. For comparison, high-quality C_{10} in which the adsorbates have a comparable molecular length can be prepared routinely by growing the films at room temperature [30].

7. Summary and conclusions

A surface diffraction study of monolayers of MMB on Au(111) has been performed. The results show that there are two ordered phases of different densities in the system, namely the striped phase and the hexagonal phase, which has a higher density. With the substrate surface lattice as a reference, the striped phase and the hexagonal phase can be described by a rectangular $(8 \times 2\sqrt{3})$ lattice and a $(\sqrt{3} \times \sqrt{3})R30^\circ$ lattice, respectively. The diffraction pattern suggests that in the striped phase the molecules orient in a head-to-head fashion, similar to the structure found for 4-mercaptopyridine on Au(111) [26], and their molecular axes are close to the surface. For the hexagonal phase, the diffraction pattern implies that the molecules pack hexagonally and assemble as thiolates. The intensity variation along the Bragg rod indicates that the molecules are tilted at most 19° from the surface normal.

This system is then compared with monolayers of *n*-decanethiol on Au(111) (C_{10}), in which the alkyl chains of the adsorbates are more flexible than the biphenyl units. The common feature of MMB monolayers and C_{10} is the existence of two ordered phases of different densities. In both low-density phases, the molecular axes are parallel or close to the surface in order to maximize the molecule–substrate interaction and the molecules are packed head-to-head. In the high-density phase, the MMB molecules are aligned closer to the surface normal instead of leaning 30° from it as in the case of C_{10}. In the standing-up phase of MMB monolayers, the S atoms occupy the $(\sqrt{3} \times \sqrt{3})R30^\circ$ positions. This is explainable in terms of the difference in the conformational freedom and the constraints of the molecular backbones of the two molecules.

The thermal behavior of both phases of MMB monolayers was also examined and compared with that of C_{10}. For the striped phase of MMB monolayers a melting transition takes place above 423 K, whereas the striped phase of C_{10} starts melting at $\sim$373 K. At 373 K, the hexagonal phase of MMB monolayers remains crystalline, whereas the hexagonal phase of C_{10} melts almost completely. The higher thermal stability of the striped phase of MMB monolayers can be ascribed to the stronger molecular backbone–substrate interaction, whereas for the hexagonal phase of MMB monolayers the thermal stability can be explained by the difference in the interface structure and in the conformational freedom of the molecules.

Finally, the growth kinetics of MMB monolayers were investigated and various growth protocols were tried. In contrast to the case of C_{10}, the high-density hexagonal phase of MMB monolayers was not frequently observed. Also, the quality of the striped phase of MMB monolayers was found to be dependent on the growth conditions. This study demonstrates the significant impact of the molecular backbone on the structures, the thermal behavior and the growth of the SAMs of thiol on gold. Also, the results underscore the need for a detailed understanding of the interplay between the various interactions present in this class of organic thin films.

Acknowledgements

The authors thank Dr A. Eberhardt and Dr P. Fenter for their help and advice in the GIXD measurements, and Professor A. Kahn and Dr G. Poirier for the STM measurements. F. Schreiber acknowledges the financial support from the DFG. A. Ulman thanks the NSF for support through the MRSEC for Polymers at Engineered Interfaces. The GIXD studies were supported by the Department of Energy under Grant No. DE-FG02-93ER45503. The GIXD measurements were carried out at the National Synchrotron Light Source, which is supported by Department of Energy Contract No. DE-AC0276CH-00016.

References

[1] A. Ulman, An Introduction to Ultrathin Organic Films from Langmuir–Blodgett to Self-Assembly, Academic Press, New York, 1991.
[2] G.M. Whitesides, C.B. Gorman, in: A.T. Hubbard (Ed.), The Handbook of Surface Imaging and Visualization, CRC Press, Boca Raton, 1995.
[3] A. Ulman, Chem. Rev. 96 (1996) 1533.
[4] P. Fenter, in: A. Ulman (Ed.), Thin Films: Self-Assembled Monolayers of Thiols, Academic Press, San Diego, 1997.
[5] A. Eberhardt, Ph.D. Thesis, Princeton University, NJ, 1996.
[6] T.Y.B. Leung, Ph.D. Thesis, Princeton University, NJ, 1998.
[7] G.E. Poirier, Chem. Rev. 97 (1997) 1117.
[8] P. Fenter, A. Eberhardt, P. Eisenberger, Science 266 (1994) 1216.
[9] J. Li, K.S. Liang, N. Camillone III,, T.Y.B. Leung, G. Scoles, J. Chem. Phys. 102 (1995) 5012.
[10] G.E. Poirier, J. Vac. Sci. Technol. B: 14 (1996) 1453.
[11] T.Y.B. Leung, M.C. Gerstenberg, D.J. Lavrich, G. Scoles, F. Schreiber, G.E. Poirier, Langmuir 16 (2000) 549.
[12] N. Camillone III, C.E.D. Chidsey, G.-Y. Liu, G. Scoles, J. Chem. Phys. 98 (1993) 4234.
[13] P. Fenter, P. Eisenberger, J. Li, N. Camillone III,, S. Bernasek, G. Scoles, T.A. Ramanarayanan, K.S. Liang, Langmuir 7 (1991) 2013.
[14] M.H. Dishner, J.C. Hemminger, F.J. Feher, Langmuir 12 (1996) 6176.
[15] W.B. Caldwell, D.J. Campbell, K. Chen, B.R. Herr, C.A. Mirkin, A. Malik, M.K. Durbin, P. Dutta, K.G. Huang, J. Am. Chem. Soc. 117 (1995) 6071.
[16] H. Wolf, H. Ringsdorf, E. Delamarche, T. Takami, H. Kang, B. Michel, C. Gerber, M. Jaschke, H.-J. Butt, E. Bamberg, J. Phys. Chem. 99 (1995) 7102.
[17] J. Li, K.S. Liang, G. Scoles, A. Ulman, Langmuir 11 (1995) 4418.
[18] R.G. Nuzzo, L.H. Dubois, D.L. Allara, J. Am. Chem. Soc. 112 (1990) 558.
[19] C.D. Bain, E.B. Troughton, Y.-T. Tao, J. Evall, G.M. Whitesides, R.G. Nuzzo, J. Am. Chem. Soc. 111 (1989) 321.
[20] G.E. Poirier, E.D. Pylant, J.M. White, J. Chem. Phys. 104 (1996) 7325.
[21] S.E. Creager, C.M. Steiger, Langmuir 11 (1995) 1852.
[22] A. Dhirani, R.W. Zehner, R.P. Hsung, P. Guyot-Sionnest, L.R. Sita, J. Am. Chem. Soc. 118 (1996) 3319.
[23] G.-Y. Liu, P. Fenter, C.E.D. Chidsey, D.F. Ogletree, P. Eisenberger, M. Salmeron, J. Chem. Phys. 101 (1994) 4301.
[24] Y.-T. Tao, C.-C. Wu, J.-Y. Eu, W.-L. Lin, K.-C. Wu, C.-H. Chen, Langmuir 13 (1997) 4018.
[25] E. Sabatani, J. Cohen-Boulakia, M. Bruening, I. Rubinstein, Langmuir 9 (1993) 2974.
[26] L.-J. Wan, Y. Hara, H. Noda, M. Osawa, J. Phys. Chem. B 102 (1998) 5943.
[27] Q. Jin, J.A. Rodriguez, C.Z. Li, Y. Darici, N.J. Tao, Surf. Sci. 425 (1999) 101.
[28] P. Fenter, A. Eberhardt, K.S. Liang, P. Eisenberger, J. Chem. Phys. 106 (1997) 1600.
[29] J.M. Tour, L. Jones II,, D.L. Pearson, J.J.S. Lamba, T.P. Burgin, G.M. Whitesides, D.L. Allara, A.N. Parikh, S.V. Atre, J. Am. Chem. Soc. 117 (1995) 9529.
[30] F. Schreiber, A. Eberhardt, T.Y.B. Leung, P. Schwartz, D.J. Lavrich, S.M. Wetterer, P. Fenter, P. Eisenberger, G. Scoles, Phys. Rev. B 57 (1998) 12476.
[31] B.M. Ocko, G.M. Watson, J. Wang, J. Phys. Chem. 98 (1994) 897.
[32] N. Camillone III, P. Eisenberger, T.Y.B. Leung, P. Schwartz, G. Scoles, G.E. Poirier, M.J. Tarlov, J. Chem. Phys. 101 (1994) 11031.
[33] N. Camillone III, T.Y.B. Leung, P. Schwartz, P. Eisenberger, G. Scoles, Langmuir 12 (1996) 2737.

[34] N. Camillone III, C.E.D. Chidsey, G.-Y. Liu, G. Scoles, J. Chem. Phys. 98 (1993) 3503.
[35] J.F. Kang, R. Jordan, A. Ulman, Langmuir 14 (1998) 3983.
[36] J.F. Kang, A. Ulman, R. Jordan, D.G. Kurth, Langmuir 15 (1999) 5555.
[37] J.F. Kang, S. Liao, R. Jordan, A. Ulman, J. Am. Chem. Soc. 120 (1998) 9662.
[38] S. Liao, Y. Shnidman, A. Ulman, J. Am. Chem. Soc. (1999) submitted for publication.
[39] A.R. Sandy, S.G.J. Mochrie, D.M. Zehner, K.G. Huang, D. Gibbs, Phys. Rev. B 43 (1991) 4667.
[40] J.F. Kang, A. Ulman, in preparation.
[41] F. Schreiber, T.Y.B. Leung, G. Scoles, in preparation.
[42] I.K. Robinson, Aust. J. Phys. 41 (1988) 359.
[43] J. Als-Nielsen, H. Möhwald, in: S. Ebashi, M. Koch, E. Rubenstein (Eds.), Handbook on Synchrotron Radiation vol. 4 Elsevier, 1991.
[44] L. Danielson, J.C. Ruiz, C. Schwartz, G. Scoles, J.M. Hutson, Faraday Discuss. Chem. Soc. 80 (1985) 47.
[45] R.A. Aziz, U. Buck, H. Jónsson, J.C. Ruiz-Suárez, B. Schmidt, G. Scoles, M.J. Slaman, J. Xu, J. Chem. Phys. 91 (1989) 6477.
[46] P. Rowntree, Ph.D. Thesis, Princeton University, NJ, 1990.
[47] N. Camillone III, Ph.D. Thesis, Princeton University, NJ, 1994.
[48] P. Schwartz, Ph.D. Thesis, Princeton University, NJ, 1998.
[49] M. Ratajczak-Sitarz, A. Katrusiak, Z. Kaluski, J. Garbarczyk, Acta Crystallogr. Sect. C: 43 (1987) 2389.
[50] G. Casalone, C. Mariani, A. Mugnoli, M. Simonetta, Acta Crystallogr. Sect. B: 25 (1969) 1741.
[51] M.M. Szczesniak, G. Chalasinski, S.M. Cybulski, S. Scheiner, J. Chem. Phys. 93 (1990) 4234.
[52] T.G. Metzger, D.M. Ferguson, W.A. Glauser, J. Comput. Chem. 18 (1997) 70.
[53] D.R. Lide (Ed.), CRC Handbook of Chemistry and Physics, CRC Press, Boca Raton, 1992.
[54] P. Fenter, F. Schreiber, L. Berman, G. Scoles, P. Eisenberger, M.J. Bedzyk, Surf. Sci. 413 (1998) 213.
[55] P. Fenter, F. Schreiber, L. Berman, G. Scoles, P. Eisenberger, M.J. Bedzyk, Surf. Sci. 425 (1999) 138.
[56] G. Casalone, C. Mariani, A. Mugnoli, M. Simonetta, Mol. Phys. 15 (1968) 339.
[57] J. Trotter, Acta Crystallogr. 14 (1961) 1135.
[58] C.P. Brock, R.P. Minton, J. Am. Chem. Soc. 111 (1989) 4586.
[59] G.J. Kluth, C. Carraro, R. Maboudian, Phys. Rev. B 59 (1999) R10 449.
[60] A. Guinier, X-Ray Diffraction in Crystals, Imperfect Crystals, and Amorphous Bodies, W.H. Freeman, San Francisco, 1963.
[61] A.I. Kitaigorodskii, Organic Chemical Crystallography, Consultants Bureau, New York, 1961.
[62] P. Fenter, P. Eisenberger, K.S. Liang, Phys. Rev. Lett. 70 (1993) 2447.
[63] P. Schwartz, G. Scoles, unpublished results.
[64] P. Schwartz, N. Camillone III, T.Y.B. Leung, G. Scoles, unpublished results.
[65] F. Balzer, R. Garlach, G. Polanski, H.-G. Rubahn, Chem. Phys. Lett. 274 (1997) 145.
[66] L.E. Firment, G.A. Somorjai, J. Chem. Phys. 66 (1977) 2901.
[67] K. Uosaki, R. Yamada, J. Am. Chem. Soc. 121 (1999) 4090.
[68] R. Gerlach, G. Polanski, H.-G. Rubahn, Appl. Phys. A 65 (1997) 375.
[69] G.E. Poirier, M.J. Tarlov, Langmuir 10 (1994) 2855.
[70] E. Delamarche, B. Michel, Ch. Gerber, D. Anselmetti, H.-J. Güntherodt, H. Wolf, H. Ringsdorf, Langmuir 10 (1994) 2869.
[71] N. Camillone III,, T.Y.B. Leung, G. Scoles, Surf. Sci. 373 (1997) 333.
[72] D.J. Lavrich, S.M. Wetterer, S.L. Bernasek, G. Scoles, J. Phys. Chem. B 102 (1998) 3456.
[73] S.M. Wetterer, D.J. Lavrich, T. Cummings, G. Scoles, S.L. Bernasek, J. Phys. Chem. B 102 (1998) 9266.
[74] S. Xu, S.J.N. Cruchon-Dupeyrat, J.C. Garno, G.-Y. Liu, G.K. Jennings, T.-H. Yong, P.E. Laibinis, J. Chem. Phys. 108 (1998) 5002.